Self-Localization Based on Visual Lane Marking Maps: An Accurate Low-Cost Approach for Autonomous Driving

Rafael Peixoto Derenzi Vivacqua, Massimo Bertozzi, Pietro Cerri,
Felipe Nascimento Martins, and Raquel Frizera Vassallo

***Abstract*— Autonomous driving in public roads requires precise localization within the range of few centimeters. Even the best localization systems based on GNSS cannot always reach this level of precision, especially in an urban environment, where the signal is disturbed by surrounding buildings and artifacts. Recent works have shown the advantage of using maps as a precise, robust, and reliable way of localization. Typical approaches use the set of current readings from the vehicle sensors to estimate its position on the map. The approach presented in this paper exploits a short-range visual lane marking detector and a dead reckoning system to construct a registry of the detected back lane markings corresponding to the last 240 m driven. This information is used to search in the map the most similar section, to determine the vehicle localization in the map reference. Additional filtering is used to obtain a more robust estimation for the localization. The accuracy obtained is sufficiently high to allow autonomous driving in a narrow road. The system uses a low-cost architecture of sensors and the algorithm is light enough to run on low-power embedded architecture.**

***Index Terms*— Autonomous driving, computer vision, dead reckoning, lane marking detector, map matching, mapping and localization.**

I. Introduction

AUTONOMOUS driving is the highest level of automation for a vehicle, which means the vehicle can drive itself from a starting point to a destination with no human intervention. While in case of aviation, this technology is quite old, in case of terrestrial vehicles, even with all the computer power available nowadays, that is just now maturing. Currently, the most important car manufacturers are publicly demonstrating the advance of their technologies, and some of them are already available for the customers.

The autonomous driving problem can be divided into two separate tasks. The first task is focused on keeping the vehicle moving along a correct path. In order to achieve this task, an accurate localization of the vehicle, with respect to the road, is a mandatory requirement. Even the most accurate positioning systems based on GNSS (global navigation satellite system), GNSS with RTK correction, GNSS and IMU fusion, or sophisticate schemes like multi-measurements in connected vehicle networks [1] still can not completely fulfil these constraints in dense urban environment. The second task is the capability to perceive and react to unpredictable dynamic obstacles, like other vehicles, pedestrians, and traffic signs.

This article is focused on the first task, the task of performing autonomous driving by tracking a pre-set route created in a manual mapping trip. We propose an accurate low-cost localization approach, combining techniques of visual lane marking detection, dead reckoning, map-matching, and data fusion. We used the monocular visual lane marking detector developed in our previous work [2], [3], originally developed to be an autonomous lane follower.

Current state-of-the art approaches use cameras or LIDAR to detect lane markings in the mid to far range (25 m), as shown in Figure 1-a. The most important novelty of the present work is a method that allows reliable and extensive perception of the lane markings (Figure 1-b), from low-cost sensors. In practice, it works as a very long range (240 m) visual lane marking detector looking to the back. The key ideas are: (i) the detection of the lane markings are performed only in a short range in front of the vehicle; and (ii) the record of the detected information is stored in a buffer, named Back Lane Marking Registry (BLMR), so it can be used for localization (see Figure 1).

The choice of detecting lane markings close to the vehicle (7.2 m) has some great advantages. For close lane marks the visual resolution is higher, and the lane markings position computation is less affected by vehicle movements, like pitch and roll, that usually dynamically affect the vision system calibration. The assumption of a flat road, used to estimate the lane markings position, is sufficiently safe when using close lane markings only. Besides that, lane markings close to the vehicle generally are not affected by occlusions. The high confidence lane markings detected immediately in front of the vehicle are stored in a registry called BLMR (Back Lane Marking Registry), and their relative position with respect to the vehicle is continuously updated by dead reckoning (see Figure 1-b). This data set accumulates the detected lane markings in a map, while the vehicle is travelling.

Manuscript received October 14, 2016; revised February 26, 2017 and July 7, 2017; accepted September 2, 2017. Date of publication October 9, 2017; date of current version February 1, 2018. The Associate Editor for this paper was P. Zingaretti. *(Corresponding author: Rafael Peixoto Derenzi Vivacqua.)*

R. P. D. Vivacqua is with the Federal Institute of Education, Science and Technology of Espirito Santo, Espirito Santo 29173-087, Brazil.

M. Bertozzi and P. Cerri are with the Dipartimento di Ingegneria dell'Informazione, University of Parma, Parma 43124, Italy.

F. N. Martins is with the Institute of Engineering, Hanze University of Applied Sciences, Groningen 9403AB, The Netherlands.

R. F. Vassallo is with the Department of Electric Engineering, Federal University of Espirito Santo, Espirito Santo 29075-910, Brazil.

Color versions of one or more of the figures in this paper are available online at http://ieeexplore.ieee.org.

Digital Object Identifier 10.1109/TITS.2017.2752461

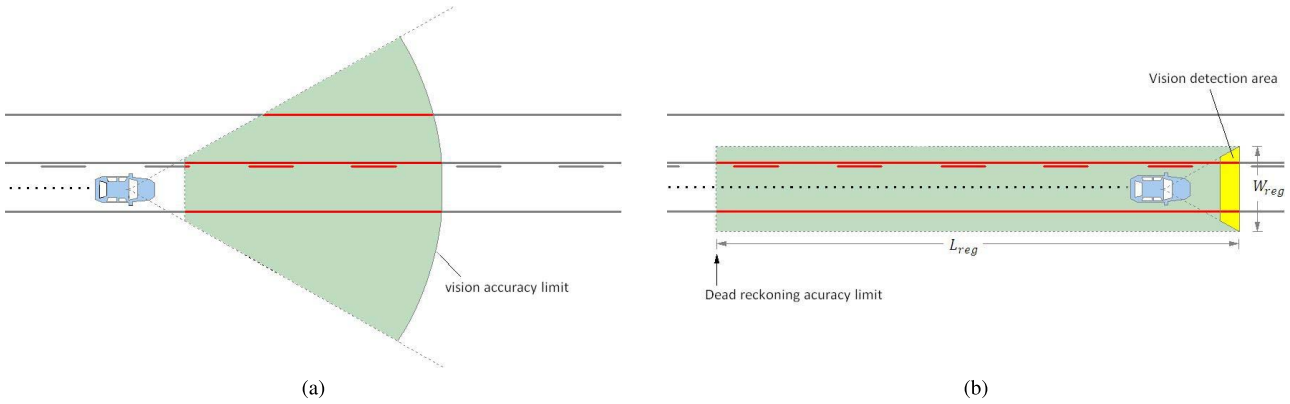

Fig. 1. (a) Typical frontal view detection with the range limited by the visual accuracy and (b) the proposed back registry with the range limited by dead reckoning accuracy.

Finally, this long and accurate BLMR perception is used for localization purpose in a map, as most state-of-the-art high-accuracy localization approaches. Despite of BLMR being generated by a cumulative process, in our approach it is treated as an instantaneous measurement and used together with gyroscope, odometry and prior road information (a map), for estimation of vehicle localization.

For building the map, the vehicle is manually driven by a person along the desired path, and a proper map is built online, not requiring any kind of post process or manual adjustment (see Figure 3). The map contains the lane markings detected and a reference path, that corresponds to the path described by the center of mass of the vehicle. The lane marking data is used for localization purpose and reference path for autonomous track following, during autonomous driving. Because the BLMR contains information of the lane markings corresponding to a long section of the road (240 m) the localization algorithm becomes more robust against sections of missing lane markings. Once the vehicle is precisely localized in the map, there is always a reference path that guides the vehicle through the sections of missing lane markings.

It is worth to mention that, differently from traditional lane followers, the new proposed system uses the road lane markings as landmarks, just for localization, not for defining a target point nor a vanishing point, usually presented in the literature as a tool for calculating the steering command for the car. It is the precise localization in the map and the map reference path that allows the computation of the steering angle.

This paper is organized as follows. Section II presents and discusses some related works in order to provide some references on the topic addressed in this work. Section III introduces the online mapping architecture and approach, Section IV describes the algorithm for the estimation of the vehicle position within the map, Section V presents results in terms of accuracy and capacity to perform autonomous driving, and, finally, Section VI ends the paper with some final remarks.

II. Related Work

Currently most successful autonomous driving projects [4]–[9] are based on accurate self-localization in mapped environment. Some of them have demonstrated the potential of this method with the realization of autonomous travels in complex real environments. In general a map contains, at least, a set of landmarks used to localize the vehicle and a reference trajectory that is guaranteed to be free of road infrastructure obstacles. If the localization technique achieves sufficient accuracy in any part of the map, the problem of autonomous driving can be reduced to a path following problem.

Very handy landmarks available in public roads are the horizontal traffic signs, like lane markings, stop lanes, zebra crossings, etc. The horizontal traffic signs have attractive advantages to be used as landmarks for localization: (i) they are widely available; (ii) they are everywhere including very near to the vehicle; (iii) they are relatively easy to detect due to the high contrast with the asphault, and (iv) they suffer little variation with time. The sensors broadly used for detecting lane markings are laser scanners (LIDAR) and cameras.

Laser scanners (LIDAR) are very suitable sensors for use in autonomous driving projects. They are capable of performing direct distance and reflectance measurements. In [5], [7], and [10]–[12] the reflectance information was used for lane marking detection. LIDAR offers great advantages, such as 360° field of view around the car and simpler data to process when compared to vision. The drawback of LIDAR is that they are expensive sensors and need to be installed on the exterior of a vehicle, often in specific positions, therefore requiring changes on the external shape of the vehicle.

Computer-vision approaches are also widely used for the detection of road and/or lane markings [5], [10], [13]–[17]. Cameras are generally small and easy to integrate into a vehicle without changing vehicle's shape. Besides that, with the exception of some devices built to acquire specific spectral ranges, like far or shortwave infrared, cameras are quite inexpensive equipment. Another interesting point is that the acquired data from a camera convey a huge amount of information. Cameras are, in fact, able to acquire texture and color of all framed objects and can also be used to estimate road surface [18], [19]. All these features make cameras a very versatile sensor that can be employed on different tasks. On the other hand, the extraction of this information requires a complex and heavy computational process. Therefore, the choice of processing engines have to take into account extra processing tasks for computer vision.

For visual localization in places without lane markings, another kind of landmarks must be used. SURF (speed up robust feature) [20] is an algorithm broadly used for detecting and describing such visual point features. For example, in [4] a visual route-following algorithm is presented for operation in off-road environments under long term light variation. The stereo vision system detects features in multiple data channels (gray scale channel and color-constant channel) to estimate map relative localization. The autonomous route following tests, performed both in summer and winter seasons, demonstrated that the use of multichannel data increases the robustness of the system against light variation. In [6] a backward vision system used SURF to detect visual features and, complement the frontal vision system based on lane markings. The use of complementary landmarks contributed to increase the localization accuracy and robustness.

As already mentioned, our autonomous driving approach is based on localization using lane marking maps. The success of this approach relies strongly on the performance of lane marking detector and the localization method. In the following we present some related work in lane marking detection and its use for localization purpose.

A. Lane Marking Detection

Lane marking detection for lateral localization and curvature estimation is one of the first research field of computer vision applied to the problem of autonomous driving, since the early '90s. Many publications and surveys were made [21]–[24] describing the diversity of techniques that were developed to solve this problem. Some of the early projects [25] already demonstrated in practice the capability of such systems in following autonomously a road for more than hundreds of kilometers. Actually, if the road has a well painted lane along all of its length, without roundabouts or bifurcations, even a simple system is capable of keeping the vehicle following the road until the vehicle's tank becomes empty.

More recently, lane marking detection regained more attention due to its commercial application in advanced driver assistance systems (ADAS) [26]–[29] for lane departure warning and lane keeping systems. Different sensors can be exploited for detecting lane markings, being LIDAR and cameras the most used. In [11] and [12] a LIDAR was used to detect lane markings, exploiting the different reflectivity between painted or bare road surfaces. In [9] frontal cameras are used to detect the preceding vehicle, in order to build the possible lane position. If the vehicle is not present, a lane marking detection algorithm is used. In [30] a simple monocular algorithm is used to detect the lane markings on the images. The position of lane markings in the world is then computed using 3D information provided by a stereo camera system using V-Disparity.

According to [31], although a vast amount of research work has already been done in lane markings detection, it is not yet completely solved and has remained as a challenging problem due to the wide range of uncertainties in real road conditions which may include shadows, variation of lighting conditions, worn-out or absence of lane markings, and other markings such as directional arrows, warning text, and zebra crossings.

B. Lane Marking Maps for Localization

Precise localization requires the construction of detailed maps containing landmarks for localization and, as already mentioned, lane markings offers great advantages. The localization process relies on the detection and position estimation of these landmarks [30], [32], [33], relative to the vehicle, and compare with information contained in a map.

In [12] a LIDAR sensor was used to measure the reflectivity intensity to detect road markings (lane markings and zebra crossings). This information was used to construct a map. Then, the Monte Carlo Localization (MCL) method was used to localize the vehicle in the resulting map. Besides the good accuracy reported (0.31m), this system has the high cost of the LIDAR sensor as a drawback.

In [34] digital maps and coherency images were used to estimate the vehicle localization. The maps are constructed from aerial images, where all the information about the lane markings and road surface are manually placed. This map is used to generate artificial images from a given point of view. A particle filter is used to estimate the vehicle position, with the likelihood of each particle being calculated from the coherency value between the current camera view and the artificial image associated to each particle. This system reported a lane-level accuracy of 0.35m, but has the disadvantage of a manual map construction.

In [32] upright SURF features are applied to extract the points which are used for both mapping and localization. This approach is described as topometric, because it is a fusion between topological and metric approaches. The localization is made on a topological map, but the map is geo-localized in order to achieve a metric localization. The method reported an average localization error of 2.70m.

In [33] 3D features, extracted using stereo vision, are used to create a 3D map in which is possible to self localize using both the real-time computed landmarks and the ones stored in the map. The reported value of mean error (0.34m) is sufficient for lane-level localization.

The authors of [13] deal with the problem of global vehicle localization applying monocular visual odometry using a single camera and a freely available digital map. Their proposed method require a pre-processing step of the digital map, and road constraints from the geometric shapes of the roads are utilized to reduce measurement uncertainties. The average error of their proposed localization method using monocular visual odometry is 5.62 m, after about 10.83 km of tests in different trajectories.

Now, in [35], an image based localization scheme was presented applying Virtual Generalizing Random Access Memory (VG-RAM) [36]. A neural map is built from 3D landmarks, detected by a stereo vision system, and used for localization. The average lateral error reported was 2.61m, which is not sufficiently small for autonomous driving.

Conversely, in [6], a combination of both front and rear camera systems is used to detect different types of landmarks.

The frontal vision system detects road elements painted on the ground (lane markings, stop lines…) to obtain a so called LFL (lane feature based localization). The rear vision system extracts a set of points features to be compared to previously acquired data, to obtain a point feature based localization (PFL) [37]. This twofold approach provides a more precise and reliable localization and allows the location system to well adapt to different road conditions of rural, highway, or urban environments. The maps is built offline using images, odometer, and GNSS data collected during a preliminary mapping trip. The successful autonomous driving performed in Germany, in a 103km length urban and rural path, demonstrated that the lateral accuracy was 0.20m in 99.9% of time.

In [5] both reflectance and distance measurements are used to build multi layer maps containing intensity and vertical features. Localization is performed using an enhanced of Monte Carlo Localization (MCL) algorithm, considering the information of each data layer and its confidence. The experimental tests performed in real urban environment demonstrated that the use of different sources of measurements resulted in better accuracy than conventional MCL fusion algorithm. The average reported error was below 10 cm.

A centimeter-level localization method is presented in [38] based on lane marking detection and maps. The lane markings are detected by a frontal camera with self-built IMU for camera pose estimation. The self-built map is a sequence of GNSS points, corresponding to the lane markings, built manually from GoogleEarth images and refined with GNSS-RTK measurements of some specific landmarks. The approach uses the GNSS/INS track and map-matching algorithm to access the prior road shape (lane markings). Then, the current lane markings presented in front of the vehicle are detected, translated and rotated, using iterative closest point algorithm (ICP) [39] to perform shape registration with the prior road shape. The result is used to correct the GNSS drift so that centimeter-level localization is achieved. The authors reported that their approach has problems when the terrain is not flat, mainly due errors in the inverse perspective transform. As explained in the following sections, our approach overcomes such problem by using back lane marking registry.

In general, current methods that achieve the highest level of precision employ heavy computational techniques, such as particle filter, computer vision for detection features (ex. SURF), or stereo vision. This requires a more powerful computer system that, along with the LASER sensor still used in many projects, leaves the final cost of the system high. Different from these approaches, the ego-localization system presented in this article is based on a short-range visual lane marking detector and a dead reckoning system, resulting in light mapping and localization algorithms. The obtained accuracy is sufficient for application in autonomous driving as demonstrated in the experimental tests.

III. Online Mapping

The online mapping is done by a prototype vehicle (Figure 2), driven by a person, along the desired path. The detected lane markings and dead reckoning data

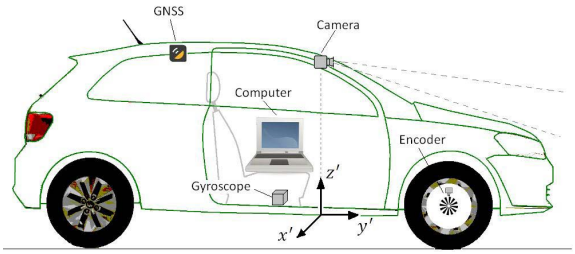

Fig. 2. Setup used for mapping and localization.

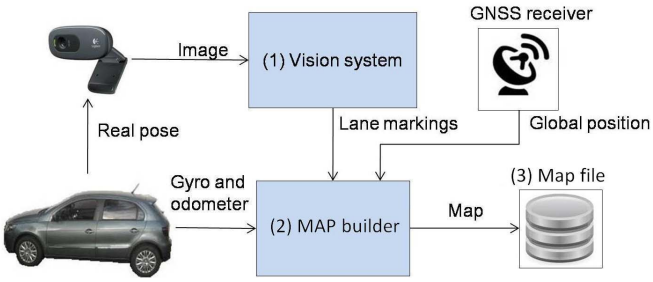

Fig. 3. System architecture during on-line mapping.

(odometer and IMU) are sampled and used to build the map. The process is completely automatic and unsupervised. During the mapping trip, the computer records the vehicle pose, estimated from 2D dead reckoning (x, y, θ) and from the lane markings positions, detected by a computer vision system.

In our tests we used two prototype vehicles, one in Brazil and other in Italy. Both equipped with: (i) a Camera to capture front images, (ii) a MEM gyroscope for yaw-rate measurement, (iii) a GNSS receiver for initial position estimation and (iv) a computer to run the vision and localization algorithms. The measurement of the longitudinal displacement (y' direction) is done by an encoder connected to the wheel, that in the case of the Brasilian car, was the original encoder used in the vehicle's speed gauge. The same setup used for mapping is also used for online localization, as explained in Section IV.

Figure 3 shows the software architecture for mapping. Module 1 is the visual lane marking detector, explained in Section III-C, that detects the lane markings relative to the vehicle's coordinate frame $(x'/y'/z')$. Module 2 uses the information from encoder and the gyroscope to calculate the vehicle's trajectory, by dead reckoning, and inserts the lane markings data after a proper conversion to the vehicle reference frame. It also associates the GNSS readings to the current vehicle pose. The output of Module 2 is a map saved in a file (Module 3).

In our approach we are not concerned about creating a map in the global reference frame (lat, lon). For this reason, the map building does not require a precise GNSS device or any kind of post processing. Each map is built in its own reference frame, where the initial vehicle pose is considered as the origin. The problem of autonomous driving mostly requires that the vehicle is positioned over a well known reference path free of obstacles, no matter where this path is. Nevertheless, raw GNSS position is considered to allow an initial position estimation.

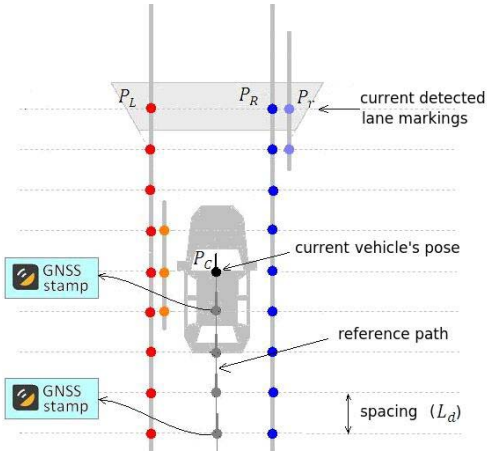

Fig. 4. Map structure and mapping example. As the car moves upward, the current pose and detected lane markings are stored according to the uniform longitudinal spacing. If GNSS data arrives, it is associated to the current pose by a GNSS stamp. The system is able to detect up to four lane markings, two for the left side ($\mathbf{P}_L, \mathbf{P}_l$) and two for the right side ($\mathbf{P}_R, \mathbf{P}_r$).

A. The Map Structure

The map structure is presented in Figure 4. It contains three kinds of data: the reference path, the lane markings and the GNSS stamps. As will be discussed in Section IV-A, the BLMR has the same structure as the map.

The reference path corresponds to the path covered (travelled) by the center of the car. It is used in the pose measurement procedure (Section IV-B) and as guide path for autonomous driving (see Figure 14). The reference path is stored as an array of vehicle's poses ($\mathbf{P}_c = (x_v, y_v, \theta_v)^T$) uniformly spaced in the longitudinal direction.

The lane markings (coloured dots in Figure 4) correspond to the lane markings detected by the vision system. The information is used only for localization purposes, as explained in Section IV-B. The data is stored as an array of four lane marking points ($\mathbf{P}_L, \mathbf{P}_l, \mathbf{P}_R, \mathbf{P}_r$) and their respective qualities. Each lane marking point contains information of position and a quality attribute. If a lane marking doesn't exist, the quality is null, if the lane marking is well painted, the quality is maximum (1.0). Every lane marking point is associated to the vehicle's pose, from where it was detected.

The uniform longitudinal spacing (L_d), used for both the map and BLMR, simplifies and speeds-up the pose measurement procedure during online localization (Section IV-B). Considering that L_d affects the matching speed and accuracy, with higher values prioritizing speed and lower values favouring accuracy, L_d was set to 1.33 m to balance these quality attributes.

B. Dead Reckoning

The calculus of the vehicle pose is made by dead reckoning technique. It is computed using the signals from the wheel encoder and a gyroscope (yaw-rate). A new pose of the vehicle ($\mathbf{V} = (x_v, y_v, \theta_v)^T$) in map coordinates is calculated every time the vehicle travels a fixed distance L_d. The state transition

Fig. 5. The visual short range lane marking detector.

expression is:

$$x_{v,i} = x_{v,i-1} + L_d \sin(\theta_{v,i-1} + \zeta_z/2) \quad (1)$$

$$y_{v,i} = y_{v,i-1} + L_d \cos(\theta_{v,i-1} + \zeta_z/2) \quad (2)$$

$$\theta_{v,i} = \theta_{v,i-1} + \zeta_z \quad (3)$$

where L_d is the fixed linear increment of 1.33 m and ζ_z is the angular variation (yaw variation) measured in the corresponding time interval. This pose serves as the basis for evaluating the position of lane markings.

It is important to emphasize that in our approach the map and also the path followed by the car do not need to be perfectly represented in the global reference frame, i.e., there is no need to be georeferenced. Instead, our algorithm builds a 2D map on its own reference frame using dead-reckoning. Then, the localization of the car is precisely determined by the BLMR algorithm (to be detailed in Section IV) on such a map. If the map does not have significant local distortions, autonomous driving is possible. By significant local distortions we mean distortions caused by a gyroscope bias greater than 1 degree per minute.

Because the BLMR algorithm was designed to be used in autonomous driving according to a predefined map, and does not need a global localization of the vehicle, we can use the BLMR algorithm to precisely localize the vehicle on its own map even with low-cost gyroscopes. According to our tests, the BLMR algorithm can cope with a drift of 1 degree per minute while maintaining a precise localization for up to 2 hours of driving.

C. Lane Marking Detector

The detection of lane markings at a fixed distance in front of the vehicle is made by a computer vision algorithm optimized for short range operation. This algorithm is a modification of the vision system used in our previous work [2], originally projected to operate up to 25 m. The short range lane marking detector (see Figure 5) uses the visual information in the range of 6.0 m up to 8.4 m to classify if there is or not a lane marking at the distance of 7.2 m in front of the vehicle. The reduced size of the region of interest (ROI) in every image frame speeds-up the processing time. Moreover the vision algorithm returns a quality factor that represents the level of confidence of this measurement [2]. The quality factor is used in the map matching calculus, as explained in Section IV-B.

The lane marking detector finds the position of the markings in the image coordinate frame. This information is transformed

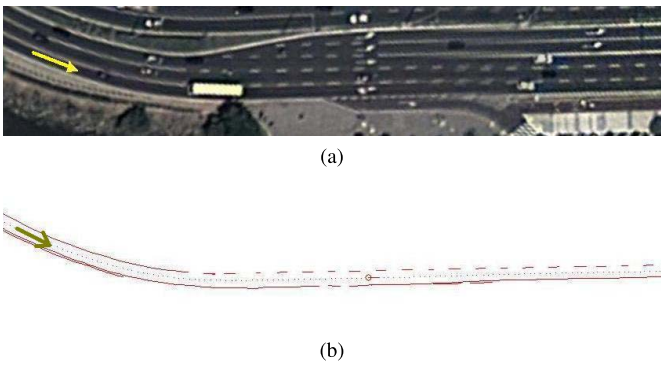

(a)

(b)

Fig. 6. Example of a Visual Lane Marking Map. (a) Satellite image. (b) Map built.

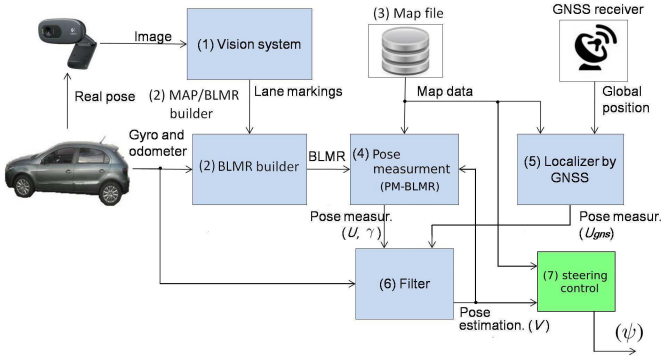

Fig. 7. The online localization architecture.

to the vehicle reference frame (x'/ y') by an inverse perspective transformation, corresponding to a bird's eye view, while considering the camera in the origin (Figure 4).

Now, the change from the vehicle coordinate frame to the map coordinate frame is made by a rotation and translation operation. Any point of a lane marking ($\mathbf{P}'_{lane}$) in the vehicle coordinate frame has its corresponding position ($\mathbf{P}_{lane}$) in the map coordinate frame computed by:

$$\mathbf{P}_{lane} = \mathbf{P}_c + R_{\theta_v}.\mathbf{P}'_{lane}, \tag{4}$$

where $\mathbf{P}_c$ is the vehicle position at the time of capturing the image, R_{θ_v} is a rotation matrix around the z'-axis by an angle θ_v, and θ_v is the vehicle orientation (heading) at the time of capturing the image. Figure 6 shows a stretch of a map generated according to the method presented in this section.

IV. Online Localization

The localization system has the function to estimate the vehicle's pose ($\mathbf{V}$) in the map reference system using two techniques of absolute pose measurement, one based on GNSS data and other based on BLMR data. This information and dead reckoning are fused by a filter to produce a continuous and more robust pose estimation.

Figure 7 shows the software architecture for online localization. Modules 1 and 2 are the same used in mapping (see Section III). Module 3 is the map, generated in a previous mapping trip, and saved in a file. Module 4 and 5 perform instantaneous pose measurement. Module 6 calculates the vehicle pose estimation (V), filtering and combining the pose measurements (U or U_{gns}) with dead reckoning data (incremental displacement). Module 7, in green doesn't belong to the localization system. It is responsible for calculating the steering wheel angle (ψ), based on the current pose and the reference path contained in the map.

The pose measurement by GNSS data is performed by Module 5 of Figure 7. It is active only during the initialization, to provide the approximate initial pose of the vehicle in the map reference system. The current global position measurement, provided by the GNSS receiver, is used to find in the map the GNSS stamp that has the shortest distance. The pose associated to this stamp is set as the initial pose ($\mathbf{V} = \mathbf{U}_{gps}$).

The pose measurement by BLMR data is performed by Module 4 of Figure 7. It is used during autonomous driving operation and, because of it, high precision is achieved. The principle, illustrated in Figure 8, is relatively simple: a pose measurement is performed by finding the pose ($\mathbf{U}_{blm}$), in the map reference frame, that results in the best matching between the lane markings stored in the map and the BLMR lane markings captured during the current vehicle trip. The overlapping (map-matching) is quantified in terms of the mean value of lateral deviation, as explained in Section IV-B.

The filter (Module 6 of Figure 7) fuses information from the absolute pose measurements with dead reckoning to produce a continuous and more robust pose estimation ($\mathbf{V}$). Basically it is a low pass filter, with different gains for lateral, longitudinal and heading components, and uses the odometer and gyroscope to compute incremental displacement (state prediction). Note that the only necessary information for autonomous driving is the pose estimation ($\mathbf{V}$), provided by the filter, and the reference path, provided by the map.

A. The Back Lane Markings Registry (BLMR)

The BLMR can be understood as a wide (long) perception of the lane markings in the vicinity of the vehicle, starting 7.2 meters in front (because the lane marking detection is frontal) and extending 240 m backwards. This concept is the core of our localization algorithm, what allows very precise pose measurement in the map reference system. This long and narrow perception (restricted to the lane width) is possible because of the combination of dead reckoning and short range visual lane marking detector. In our approach, this long perception (the BLMR) acts like a single instantaneous sensor reading, used for localization purposes.

The BLMR is constructed exactly the same manner as a map. In fact it is a piece of a map. The difference is that it has its own coordinate frame (x', y'), with the origin fixed on the center of the vehicle ($\mathbf{U}' = [0, 0, 0]^T$). The other difference, of course, is the limited number of samples. The upper bound box of Figure 8 illustrates an example of BLMR.

Finding the ideal BLMR lenght is not an easy task to be done. The longer it is, the more information it contains, what is good to improve the accuracy pose measurement. On the other hand, dead reckoning accumulates error that degrades the confidence of farther data. We chose the value of 240 m for the BLMR by a trial process using experimental data logged

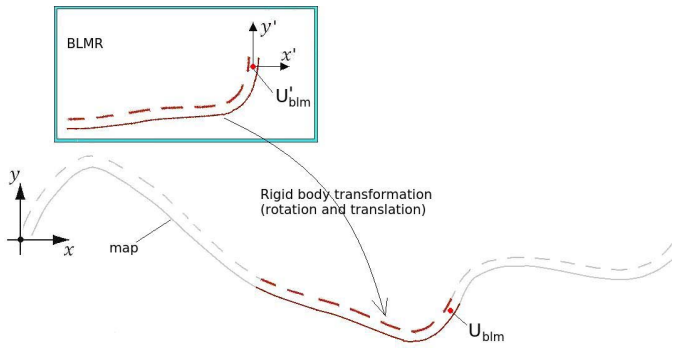

Fig. 8. Pose measurement strategy: find the rigid body transformation that results in best matching of BLMR lane markings and map lane markings.

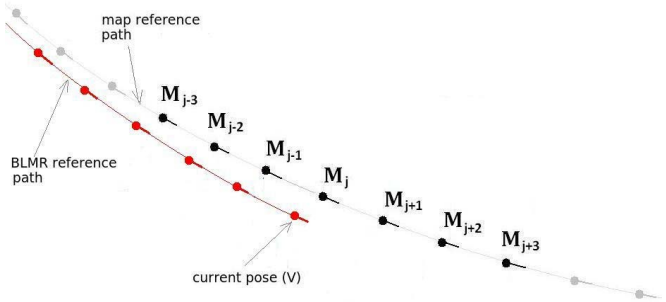

Fig. 9. Candidates head points (**M**) selected as the nearest to the current vehicle pose (**V**). The lane markings were omitted only to simplify the drawing.

by the prototype vehicle. We experimented values in the range of 60 m to 540 m, and chose the one that produced the highest accuracy, according to the criteria described in Section V-A.

B. Pose Measurement

The pose measurement by BLMR map-matching (PM-BLMR) is an algorithm that provides single pose measurements, by finding the optimal rigid body transformation (rotation and translation) that best matches the BLMR lane markings to the map lane markings. It is a classical problem of registration of shapes, whose principle is illustrated in Figure 8. Once the best transformation is found, the pose measurement is given by transforming the vehicle's pose, in the BLMR reference frame ($\mathbf{U'}_{blm}$), to the map reference frame ($\mathbf{U}_{blm}$). Note that the pose measurement is not used directly for autonomous driving, instead it is used only to update the vehicle's pose estimation, computed by the filter (Module 6 of Figure 7). Note also that the reference path data doesn't participate in the matching computation. This is because the exact path driven during manual drive and autonomous driving can be slightly different.

The best match transformation between two sets of 2D points can be found directly by any shape registration algorithm. Iterative closest point algorithm (ICP) [39] is a powerful and consolidated algorithm capable of performing 2D or 3D shape registration of a wide variety of geometric data (points set, line segments, implicit curves), without prior knowledge of the data correspondence. Currently there are many variants of basic ICP, some adopting particular strategies for selecting source points, weighting the correspondences pair and outliers rejection. ICP requires a starting transformation that must be chosen carefully to guarantee that the solution will not be trapped in a local minimum. In our case (BLMR and map), as the point correspondence between BLMR and the map is almost known, we developed a simple and lightweight matching algorithm, optimized to the particularities of our data structure.

In the case of BLMR and the map, as they are generated in accordance with the same longitudinal sample spacing, if we establish the correspondence to the first point (head point - $\mathbf{U}_{blm}$), automatically the correspondence will be established to all other points (see Figure 4). After point correspondence is done, the best rigid body transformation can be found straightforward. In our approach, the process of establishing the correspondence to the head point is made by trial and error verification, searching for the correspondence that results in the minimum matching error (best matching). As the current vehicle's pose estimation (V) is available from the filtering module, we simply pick the 7 nearest map points (Figure 9) to use as head candidate points. Note that the lane markings were omitted only to simplify the drawing. Note also that as the candidates head points are longitudinally distributed, finding the best candidate corresponds to solve the longitudinal component of pose measurement.

As mentioned before, if point correspondence between two points sets is known, the best rigid body transformation that minimizes the quadratic error can be find. In [40] a closed form solution is presented based on unit quaternions. The translation is calculated by the difference between the center of mass of the two data sets, and the rotation is calculated by the singular value decomposition (SVD) of the covariance matrix.

In our case, besides the uniform longitudinal spacing, our data set has other particularities: (i) the data is geometrically elongated, i.e. the bound box that contains the BLMR data has high height/width ratio. (ii) each lane marking point has a confidence factor (quality factor - see Section III-C) attributed by the visual lane marking detector. (iii) due to the dead reckoning calculation used in the generation of BLMR, the points near to the head point have higher confidence than the points that are further away.

In order to the keep the overall localization algorithm lightweight, we proposed a customized fast algorithm to find the rigid body transformation without solving the costly SVD decomposition. Our algorithm is divided in two steps. First translation and rotation are calculated using the reference path data. Second, lateral fine adjustment is applied using the lane marking data. After that, the matching error is calculated using lane marking data, considering de quality factor of each lane marking point and a confidence factor due to dead reckoning uncertainty. Finally the analysis of the matching error graph is performed to generate a confidence parameter for longitudinal measurement.

The rigid body transformation steps are detailed below:

1) Translation and Rotation: Translation and rotation are performed directly with information retrieved exclusively from

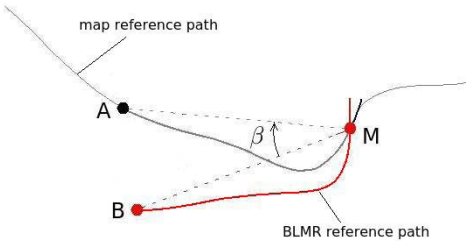

Fig. 10. Heading adjustment: calculus of the rotation angle β to align vectors MA and MB.

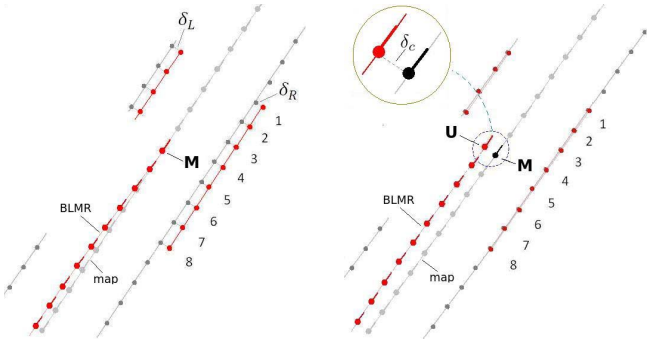

Fig. 11. Lateral adjustment: (a) Calculus of lateral offset; (b) After lateral shift of BLMR.

the reference path of the map and the BLMR. This process corresponds to a first approximation of the rigid body transformation. First the BLMR is translated so that point **U**'coincides with the candidate point, than a rotation is performed so that the vector MA has the same direction as MB (see Figure 10).

The rotation angle β is computed by the expression:

$$\beta = \arcsin\left(\frac{|\vec{MA} \times \vec{MB}|}{|\vec{MA}||\vec{MB}|}\right) \tag{5}$$

2) Fine Lateral Adjustment: The fine lateral adjustment corresponds to the second approximation to find the rigid body transformation. This process measures the most critical information for autonomous driving, the lateral displacement. The fine lateral adjustment is done according to the scheme illustrated in Figure 11-a. The objective is to calculate the necessary lateral translation that results in minimum lateral difference between the map lane markins and the BLMR lane markings.

This adjust is computed using the 8 more recent lane marking points so that a fast response can be obtained. In the example of Figure 11-a, the left lane is intermittent and the right lane is continuous. When the four lane markings are available (R, r, L, l), all of them are used in the calculus, weighted by their quality (Q), according to equation:

$$\delta_c = \frac{\sum_{j=1}^{8} \sum_{i=[R,r,L,l]} Q_{map,i,j}\, Q_{blm,i,j}\, \delta_{i,j}}{\sum_{j=1}^{8} \sum_{i=[R,r,L,l]} Q_{map,i,j}\, Q_{blm,i,j}} \tag{6}$$

Finally, the lateral offset δ_c is used to translate laterally all the BLMR data (lane markings and reference path), obtaining the final result shown in Figure 11-b.

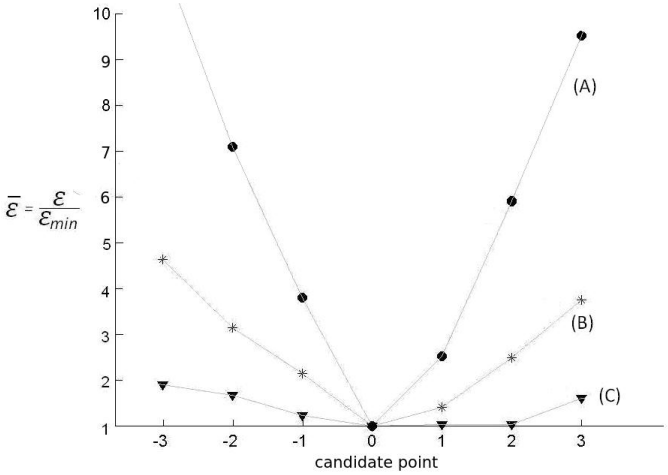

Fig. 12. Matching error (normalized) for different sections of our experimental real world data: (A) the BLMR contain a sharp curve; (B) the BLMR contain a medium curve; (C) the BLMR is nearly a straight line.

After obtaining the rigid body transformation associated to each candidate head point, the matching error is calculated for all of them. Figure 12 illustrates the normalized matching error graphs computed in three different sections of our experimental data. The final rigid body transformation considered is, of course, the one with smaller matching error.

The matching error is computed as the average value of the lateral deviation (absolute value) between the corresponding samples of BLMR lane markings and map lane markings. The weighting factor considers the higher uncertainty of further samples (caused by dead reckoning). It is computed by $G_j = exp(-(\frac{j}{n})^2)$, where n is the number of BLMR samples (n = 180). The matching error is calculated as:

$$\varepsilon = \frac{\sum_{j=1}^{n} G_j \sum_{i=[R,r,L,l]} Q_{map,i,j}\, Q_{blm,i,j}\, |\delta_{i,j}|}{\sum_{j=1}^{n} G_j \sum_{i=[R,r,L,l]} Q_{map,i,j}\, Q_{blm,i,j}}, \tag{7}$$

where $Q_{map,i}$ is the quality of the i-th map sample; $Q_{blm,i}$ is the quality of the i-th BLMR sample; $|\delta_{i,j}|$ is the absolute lateral deviation.

Analysing the slope of the matching error graph (Figure 12) we can extract various information regarding the BLMR shape and how it affects the confidence of choosing the best head point (discrimination of the minimum error point). Graph A corresponds to a section of the road that contains a sharp curve, so a small longitudinal shift of BLMR over the map (variation of head candidate point) causes much variation in matching error (highly discriminative). In this case it is very easy to identify the minimum of the graph, which results in high confidence of longitudinal pose measurement. On the other hand, graph C corresponds to a section nearly straight. In this case, longitudinal shifts causes very small variation in the matching error, what reflects low confidence in pose measurement. Graph B is an intermediate case.

In order to model this uncertainty so that it can be used by the filter, we proposed the mathematical relation illustrated in Figure 13, where (γ) is the confidence parameter and ($max(\bar{\varepsilon})$) is the maximum value of the normalized matching error. We established two threshold values for $max(\bar{\varepsilon})$.

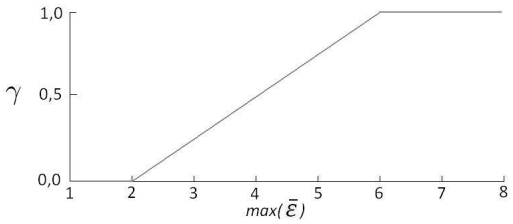

Fig. 13. Confidence parameter for the longitudinal pose measurement.

When it is smaller than 2, we considered that the BLMR is too straight, and the confidence parameter is null. When it is greater than 6, we considered that the BLMR contains sufficient curvature so that the confidence parameter is maximum.

C. Filter

The filter (Module 6 of Figure 7) is responsible for generating a continuous and smooth estimation of the vehicle's pose ($\mathbf{V}$). The filter reduces the noise (random error) of the absolute pose measurement (provided by the PM-BLMR module) and fuses it with data from gyroscope and odometer. Bayes Filter is a probabilistic filtering technique widely used in mobile robot (vehicles) localization. Bayes filter requires that measurements follow a Markov process assumption for the independence of each unit of time, so it is not appropriate to PM-BLMR once the BLMR is a temporal accumulation of road surface marking detection. We proposed a simple non-probabilistic filtering approach (we don't estimate the probability density function) that doesn't require Markov process assumption. It is based on a first order low-pass filter with independent update gains for each component of pose measurement (k_c-lateral, k_l-longitudinal and k_h-heading). Because of particularities of the PM-BLMR algorithm, we opted to set the lateral and heading gains as fixed and, the longitudinal gain as adjustable according to the confidence parameter γ.

As discussed in the previous section, the longitudinal pose measurement (choice of best candidate point) is a process whose error (confidence of measurement) depends on the shape of the BLMR. To take the confidence into account in the filtering process, we use the confidence parameter (γ). This parameter acts directly in the longitudinal update gain through the expression.

$$k_l = \gamma\, k_{lmax} \tag{8}$$

where k_{lmax} is the maximum value of longitudinal filtering gain.

When the BLMR is almost a straight line, the confidence parameter γ is null, so no update in the longitudinal localization will be done. On the other hand, when the BLMR contains sharp curves, the confidence parameter γ will be nearly one, so the update will be performed with the maximum value of gain (k_{lmax}). Moreover, the longitudinal pose measurement is restricted to the longitudinal uniformly spaced structure of the map (see Figures 4 and 9), which adds high-frequency discretization noise to this component.

To properly filter out the high-frequency spatial noise contained in the longitudinal pose measurement, and produce a continuous and smooth longitudinal pose estimation, we set the maximum update gain (k_{lmax}) to a low value (slow filter action). The slow update action for the longitudinal pose estimation is not a problem because it is much less important than the lateral component to keep the car in the center of the road, when performing autonomous driving. Moreover, as the car is being driven in a paved road (where tire slippage is minimal), the cumulative error in the longitudinal direction grows very slowly so that slow update action is enough to keep the longitudinal slippage error limited.

Lateral pose estimation is the most critical information when keeping autonomously the vehicle in lane. So a fast response is required. Moreover, the lateral measurement, performed by the short-range lane marking detector, produce small values of error. Because of this, we set the value of the gain for this component much higher then for the longitudinal component. Regarding the heading gain, heading measurements generated by PM-BLMR are quite stable and, therefore, a fast filtering action can be used, just as in the case of the lateral component. The update of the vehicle state is done by equations 9 to 11, every time a new sample is introduced in the BLMR.

$$\mathbf{V}_i = \mathbf{V}_{i-1} + R_\theta K R_\theta^T (\mathbf{U}_i - \mathbf{V}_{i-1}) \tag{9}$$

$$R_\theta = \begin{bmatrix} \cos V_\theta & -\sin V_\theta & 0 \\ \sin V_\theta & \cos V_\theta & 0 \\ 0 & 0 & 1 \end{bmatrix} \tag{10}$$

$$K = \begin{bmatrix} k_c & 0 & 0 \\ 0 & k_l & 0 \\ 0 & 0 & k_h \end{bmatrix} \tag{11}$$

where K is the gain matrix for the separated components, and R_θ is a matrix that operate a 2D rotation only in the x-y components.

The initial values for the gains were set to $k_c = 0.1$, $k_l = 0.01$, and $k_h = 0.1$. These values were then fine tuned during experimental tests and we noticed that the best results were achieved with $k_c = 0.25$, $k_l = 0.008$, and $k_h = 0.25$.

Before the filter starts to operate using the precise pose measurements from PM-BLMR, it must go through three operation modes. First, a raw localization must be provided by the GNSS. Second the system must waits until the BLMR be filled up so that the PM-BLMR be possible. Finally, when the BLMR is completly full, the filter starts to work on the precise mode. Note that in all filtering modes dead reckoning is used to predict the vehicle's pose.

1) Mode 1 - Unknown Localization: The first mode is active when the filter has no estimation of the vehicle position, i.e. when the system is turned on. When the vehicle starts to move, the BLMR builder module starts to store the samples. Thus, when the GNSS receiver becomes active, the localization module (Figure 7) finds the nearest position ($\mathbf{U}_{gns}$) in the map, using the GNSS stamps information (Figure 4). The filter considers this point as the first estimation of the vehicle localization and sets its state to this value ($\mathbf{V}_0 = \mathbf{U}_{gns}$). After that, the filter switches to Mode 2.

2) Mode 2 - Approximated Localization: In this mode the filter waits the BLMR reaches its minimum operational length (1/2 of maximum length). When this occurs

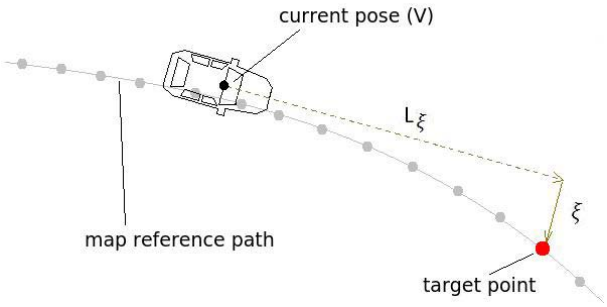

Fig. 14. Autonomous drive based on following a forward target point on the reference path.

the PM-BLMR module enters in operation and, if the matching error obtained is smaller than the threshold value (0.5 m), the filter sets this measurement as current filter state ($\mathbf{V}_0 = \mathbf{U}_{blm}$), and switches to operate in precise mode (Mode 3). While is in this mode, the filter continues to use measurements from GNSS to update the filter state.

3) Mode 3 - Precise Localization: The third mode is activated after localization by BLMR enters in operation, as explained in the previous mode. Now, the localization system does not use the GNSS anymore. The localization is updated exclusively from the measurements made by the BLMR localization module. Only in this mode the vehicle can perform autonomous driving.

V. Tests and Results

The evaluation of the localization system was performed in two parts. The first part of the tests was made in Brazil, with the objective of analysing the localization accuracy of our method. The second part of the tests was made in Italy, with the objective of verifying the performance of autonomous driving based on our localization method. At the end of this section we also present the computational performance of the algorithm.

A. Localization Accuracy

The calculus of localization accuracy of vehicles operating in real road conditions is a complicated issue due to the practical difficulty of obtaining the ground truth. Normal GNSS system cannot be used because its own error is much bigger then the expected error for the investigated method. High precision GNSS systems, like GNSS with RTK correction, could be used in some special circumstances.

Our localization algorithm was designed mainly for autonomous driving purposes, one of the applications that requires the highest level of localization accuracy and reliability. So the methodology used to calculate the accuracy was concerned in the information that affect directly this task.

One simple manner to perform autonomous driving is to use the lateral deviation of a target point (ξ), in relation to the vehicle longitudinal axis, to compute the angle of the steering wheel position (Module 7 of Figure 7) [2], [25]. The idea is illustrated in Figure 14. The radius of curvature, and consequently the steering wheel angle (ψ), necessary to make the vehicle reach the target point, is calculated by expressions 12 and 13, where f is a function of the kinematic parameters of the vehicle.

$$R(\xi, L_\xi) = \frac{\xi^2 + L_\xi^2}{2\xi} \tag{12}$$

$$\psi(\xi, L_\xi) = f(R) \tag{13}$$

For a given distance L_ξ, the lateral deviation ξ can be accessed from the current vehicle state ($\mathbf{V}$), provided by the filter, and the map reference path, recovered from the map file. Note that the only variable susceptible to uncertainty, that inserts random error in the computed steering angle (ψ), is the variable ξ. For this reason, we proposed a method to evaluate the accuracy of localization analysing the error of the variable ξ (lateral error of the target point - LETG).

The distance L_ξ, used in the analysis, is fixed and was chosen considering the speed of 60 km/h for the mapped section, and the time-to-reach of 1.5 s. The target point is taken directly from the map reference path (Figure 14), choosing the one whose distance is closer to L_ξ.

The data used for the calculus of accuracy was collected from two roads with different geometric characteristics (see Figure 15. The total data collected in those roads, in 21 trips, corresponds to 177 km. We didn't choose a highway for the tests because, despite the excellent painted signalization, normally it contains few and very smooth curves, what, as explained in section IV-B, makes the longitudinal localization more difficult.

The first road is located in the city of Vitoria, ES, Brazil (S20.2971567, W40.2920133) with total length of 5.1 km. It is a wide (three lanes in each direction) urban avenue, localized at the sea shore, in very flat terrain with few and smooth curves. The mapping trip and the first two localization trips were made on the same day, under similar lighting conditions (a cloudy day). Two localization trips were made 15 days later, also on a cloudy day. Finally, the last two localization trips were made one month after the first, with clear blue sky.

The second road is located in the city of Venda Nova do Imigrante, ES, Brazil (S20.348685,W41.1297919) with total length of 12.2 km. This road presents a much more complex geometry then the first. It is a rural road with more curves, sharper curves and curves in slope. The tests in this road were performed in both directions. The first three localization trips were made one day after the mapping trip, in a cloudy day. Then two more trips were made, two days latter, in a rainy day.

The protocol for calculating the accuracy is described as follows:

- First, the prototype vehicle was manually driven along the desired path, to build the map.
- Exactly like before, more trips were made, simulating the autonomous driving trips. The data was saved in file for offline analysis.
- The localization program processed offline the recorded data and calculated the accuracy, presented as the violin plots of the absolute value of LETG.

(a)

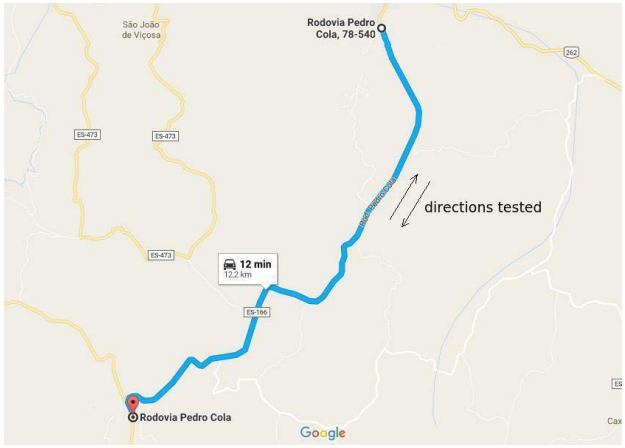

(b)

Fig. 15. Roads used for calculus of accuracy. (a) Test road 1 (6 × 5.1km). (b) Test road 2 (6 × 2 × 12.2km).

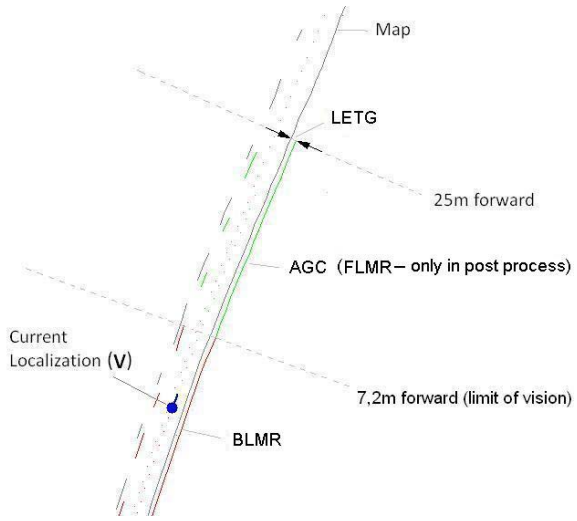

Fig. 16. Dead reckoning registry for estimation of the lateral error of the target point (δ_ξ).

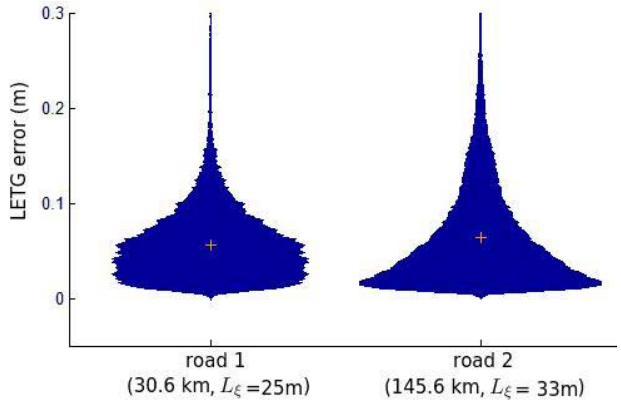

Fig. 17. Localization accuracy: Violin plots (vertical histograms) of the lateral error of target point (LETG) of two tested roads. The cross corresponds to the mean value.

1) Ground Truth Computing: To calculate the error of ξ (LETG), it is necessary to compare it with a reference true value. In our case the error is calculated in relation to an almost-ground-truth (AGT) reference. The computation was made in post processing, where the records of dead reckoning were available for the entire trip. Therefore we used this information to reconstruct the position of the lane marks 25 m in front of the car, considering this as AGT (Figure 16). This information corresponds to the "forward lane marking registry" (FLMR). Based on experimental analysis of our dead reckoning system, the lateral error introduced by it, in the range of 25 m, is only 1.2 cm (0.05%). Another source of error that affects ξ is the random variation of the vehicle's pitch angle due to the movement on an imperfect surface. Based on the parameters of the inverse perspective transform, and the measured pitch variation taken with x'-axis gyroscope, we estimate this parcel of error around 2.0 cm. So, we consider that the AGT has an inner error of 2.33 cm in relation to the exact ground truth, what is perfectly acceptable, in our case.

The LETG, was obtained directly from the lateral difference between the AGT and the map lane markings, calculated at the distance (L_ξ) ahead.

2) Results and Discussion: Figure 17 shows the violin plots (vertical histograms) of the absolute value of the lateral error of the target point (LETG), obtained from each tested road. It represents the error distribution of our autonomous driving variable ξ.

For road 1 was considered the operation speed 60km/h, and the target point 25 m ahead.The average value obtained for the error is 0.056 m and is below 0.290 m for 99.9% of the route. The corresponding angular errors, computed according to $\frac{\delta_\xi}{L_\xi}$, are 0.13° and 0.66° respectively. For road 2 was considered the operation speed 80km/h, and the target point 33 m ahead.The average error obtained is 0.064 m and is below 0.410 m for 99.9% of the route. The corresponding angular errors, computed according to $\frac{\delta_\xi}{L_\xi}$, are 0.11° and 0.71° respectively. The low values of LETG obtained after processing 177km of real data, from two different roads, are an strong indicator that the system is capable of performing autonomous driving successfully. This encouraged us to go on to the autonomous driving test, presented in the next section.

The mean LETG values obtained for the two roads were very close, with the LETG of road 2 being slightly higher then road 1. This difference was expected because the target point for road 2 is placed further from the car. But note that for

TABLE I
SUMMARY OF RESULTS REPORTED IN SOME ONLY-VISION LOCALIZATION APPROACHES

	Our approach	*[12]*	*[6]*	*[32]*	*[33]*	*[38]*	*[35]*
Localization method	back lane marking registry (BLMR) map-matching and variable gain filtering	monte carlo (MCL)	three methods were used: (i) minimization of especific error function (for PFL); (ii) kalman filter (for LFL) and; (iii) sigma-point Kalman filter (fusion of PFL and LFL).	discrete bayes filter	3D features map-matching	iterative closet point (ICP)	virtual generalizing random access memory weightless neural networks (VG-RAM)
Online localization	yes @ 130Hz	not declared	yes @ 10Hz	no	yes @ 17Hz	yes @ 20Hz	no
Ground truth (device or method)	map relative - post process of dead reckoning	Xsens MTi-G GPS device	map relative	standard GPS	high precision DGPS	manually labelled lane markings	repetibility (comparison between two trips)
Ground truth (acuracy)	0.02m (because dead reckoning)	no reported	0	reported 3.0 m	no reported	no reported	0
Error (method)	lateral of target point (LETG)	lateral/longitudinal /total	lateral	total	total	lateral by distance ranges. (range displayed here is 20m-30m)	total
Error (mean)	0.063 m	0.31m / 1.20m/ 1.25m	0.100m	2.70m	0.340m	3 pixels (0.150m)	2.61m
Error (max in 99.9%)	0.401m	-	0.200m	no reported	no reported	no reported	no reported
Error (max in 100%)	0.540 m	1.50m / 0.75m / 1.40m	no reported	18.0 m	no reported	no reported	6.50m
Autonomous driving validation	yes	no	yes	no	no	yes	no
Total lenght of tests	6 x 5.1km + 12 x 12.2 km = 177km	2 x 0.82km = 1.64km	103km	1 x 8.8km = 8.8km	2 x 1km = 2km	Tested in FC2011 contest (autonomous car competition in china)	2 x 3.57km = 7.14km

the angular error occurred the opposite. It is worth to mention that the LETG distribution will vary depending on the shape of the mapped path (geometric characteristics). LETG can be caused by: (a) error in the visual process of lane marking detection; or (b) longitudinal error of localization.

The LETG due to the lane marking detector is caused by the variation of the pitch angle (a natural movement while the vehicle moves), random deficiencies in the painted lane markings and internal noise of the lane detection algorithm. It occurs uniformly in the entire path, regardless of being on a straight path or curve. It acts as a background noise, what explains why most of LETG is concentrated in the range (0 - 0.1 m).

In turn, the LETG caused by the longitudinal localization error occurs only in the beginning of curves. For example, consider that the vehicle is in the beginning of a curve after a long straight. Due to the impossibility of a precise longitudinal localization in the straight section, longitudinal localization error may occur. Suppose that the vehicle is in advance in the map, which means in this case that, it "thinks" the curve will start earlier than it will in fact. This will cause a momentary high value of LETG. When the car starts to perform the curve, the curvature information enters in BLMR what permits the longitudinal localization to be correctly updated. But during this transition time there will be a great value of LETG. This explains the greater (but low frequent) values of LETG in the histogram ($>$0.1 m). Note that the sharper the curve the greater the LETG.

Finally, as different roads have different quantities and intensities of curves, the distribution of this parcel of LETG will vary.

Table I presents a summary of our accuracy results and other state-of-the-art vision-based localization approaches. Note that different approaches use different methodologies to calculate the localization error, so numerical comparison should be done with caution. Some works reported every error component (lateral, longitudinal and total), others reported only the total.

Fig. 18. Test vehicle used in the autonomous driving tests.

The LETG error function proposed in this work combines both longitudinal, lateral and heading errors in a manner that they affect directly the autonomous driving accuracy. On the other hand, some works presented in the table provided only the mean error, while others, the mean and maximum and, others a graph of the error over time (that we used to estimate the maximum error when it was not declared in the article text). In our case, we presented the average error, the percentile 99.9% value and the violin plots, that permits complete visualization and statistical analysis.

Note that the lateral error is more critical then the longitudinal for autonomous driving applications. Note also that a localization system can present a very low value of mean error but if, even for short periods of time, the error rises above a maximum safety limit, the system is not able to perform autonomous driving. A unquestionable way for a

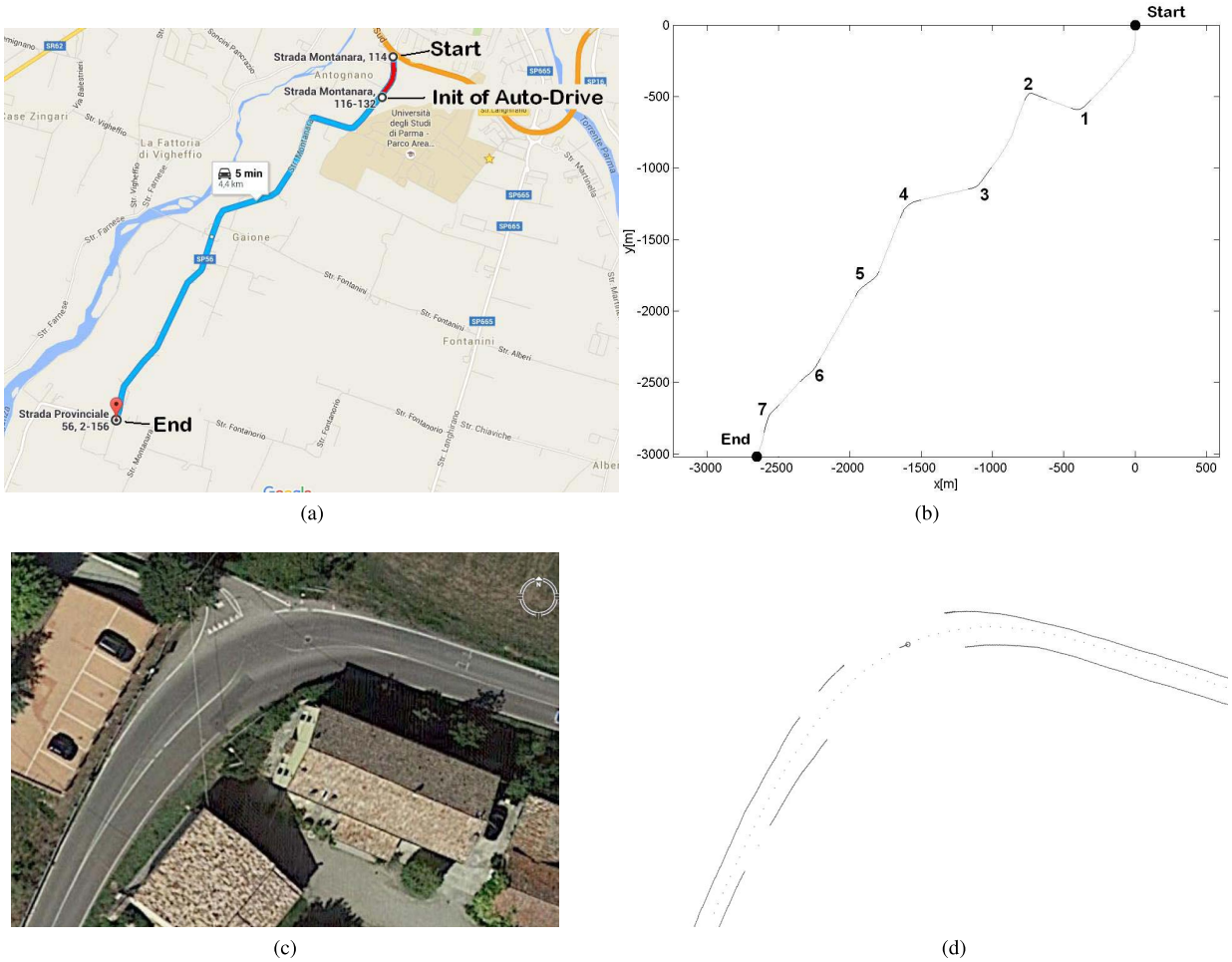

Fig. 19. The chosen road section to the autonomous driving tests: (a) map from Google Maps; (b) map build by the vehicle's dead reckoning system; (c) satellite image of curve 2; (d) lane markings detected by the vehicle's vision system in curve 2.

high accuracy localization system demonstrates its capacity is through the realization of autonomous driving tests in complex and varied public roads. The safety realization of such tests is an expensive, complex and time costly task, assumed only by a small part of the related works.

All the experimental data collected by the test vehicle in Brazil (maps according to the structure described in section III-A) are available in http://bit.ly/1MH1Pqb. Moreover we included a MATLAB script file to access the raw data of the computed LETG so that other kind of statistical analysis can be performed by anyone who is interested.

B. Autonomus Driving

Once the localization system demonstrated good accuracy, we set off for the autonomous driving tests. The tests were performed in Italy, supported by the VisLab laboratory from the University of Parma. The tests were made with the vehicle named PORTER, shown in Figure 18. This vehicle is one of the four that participated in the VisLab Intercontinental Autonomous Challenge [9], in 2011. PORTER has a servo motor to act on the steering wheel and was modified with the installation of the same hardware architecture of the Brazilian vehicle so that it could run the BLMR localization algorithm.

1) Mapping Trips: The place chosen to be mapped was a strech of 4.4 km of Strada Montanara, located in the neighborhood of the University of Parma (Figura 19-a), starting at the coordinate N44.773166; L10.307766. Because it is a country road, narrow, two-way and crossing an urban stretch, we considered it complex enough to rigidly evaluate the performance of the BLMR algorithm.

Two mapping trips were performed, and the resulting map produced by one of them is shown in Figure 19-b. The gray line represents the exact path where the vehicle was driven during mapping, i.e. the reference path to be used as a guide when operating in the autonomous driving mode. The curves are highlighted in black and numbered. Figure 19-c shows the satellite image of the curve 2 and Figure 19-d the corresponding built map. Because it has a small radius, and there are no lane markings exactly in the middle of it, we consider this curve the most challenging part to the autonomous driving algorithm.

To verify the repetitiveness of the mapping process, the comparison between the two built maps was made by map-matching the corresponding sections. The sections analyzed, enumerated in Figure 19-b, has the same length as the BLMR, or 240m. The value of the matching error represents

the average lateral difference between corresponding points of the two maps. The values obtained in centimeter were 9.4; 6.6; 5.1; 12.6; 6.4; 8.7; 2.7. This low values of errors indicated that the two build maps are very close in shape, demonstrating the good repetitiveness of the mapping system, which is a prerequisite for the proper functioning of the BLMR localization and autonomous driving method.

2) Autonomous Trips: The objective of these tests is to evaluate the performance of autonomous driving in real conditions using the method presented in this work. The steering wheel command is calculated based on the relative position of the target point to the current vehicle pose in the map coordinate frame, which is provided by the localization and map information. The instantaneous curvature required to the vehicle's trajectory is calculated according to Expression 12, that, together with the parameters of the kinematic model of the vehicle, are used to set the position of the steering wheel actuator.

We performed a total of 15 autonomous driving tests in a progressive scale of difficulty, starting with speed of 40 km/h and little traffic to the speed of 60 km/h in more traffic hours. In all trips the throttle and breaks were controlled by the driver. From the 15 tests of autonomous driving, the vehicle completed successfully 14 of them. The vehicle's behavior was smooth and stable, without any abrupt lateral movement, conveying passengers a sense of comfort and confidence.

The algorithm demonstrated robustness when faced difficult conditions like sun setting ahead, failures or absence of lane markings, crossing vehicles on narrow stretches. The only fail occurred in the 11th test, in the curve number 2, when occurred a false detection of the guardrail. It is important to remember that the algorithm presented in this article does not address the detection of moving obstacles, so in some cases human intervention was required to make a light detour to the track center to divert cyclists or cars parked on the side.

All tests were recorded by an internal camera and the camera of the vision system. Figure 20 shows a sequence of photos taken in one of these tests, and the complete video can be accessed at https://youtu.be/i9UNKuL5V8E.

Fig. 20. Photos inside the test vehicle performing autonomous driving.

TABLE II
COMPUTATIONAL PERFORMANCE: TIME SPENT IN EACH PROCESS OF THE LOCALIZATION SYSTEM

#	*Process*	*Time* (ms)
1	Lane markings detection	3.90
2	BLMR Building	0.01
3	Pose measurement (PM-BLMR)	2.38
4	Filtering (prediction and update in Mode 3)	0.37
5	Other	1.00
	Total	7.66

C. Computational Performance

The analysis of the computational performance of the localization algorithm was made in terms of time spent to process each step in a specific computer. The objective of this analysis is to have a rough idea of computational weight of the implemented algorithm, in order to verify the possibility of implementing it in smaller and cheaper computer systems. A laptop with a processor Intel Celeron 1.86 GHz was used. Table II shows the time spent on each step of the localization algorithm.

Considering the time spent on a modest computer to run the visual lane marking detector and the localization tasks, the value of 7.66 ms demonstrates that our approach is computationally very lightweight. This computational performance was possible because of the efforts given to every step during the system conception, including the choice of the sensors, the implementation of a customized computer vision algorithm for lane marking detection, the choice of an efficient map structure, the PM-BLMR fast algorithm, and the light filtering approach. We consider that the high-accuracy obtained from such a lightweight algorithm and low-cost hardware is the major contribution of this work.

VI. CONCLUSIONS AND FUTURE WORK

This paper presents a novel low-cost high-accuracy localization method for outdoor vehicles capable of performing autonomous driving in narrow two way roads. The approach is based on the Back Lane Markings Registry (BLMR) and a lightweight method of data matching and filtering. The key idea is the BLMR, a precise reliable and extensive perception of the lane markings in the vicinity of the vehicle, constructed from a monocular frontal and a dead reckoning system. The BLMR data is used to measures the vehicle pose (PM-BLMR),

in the map frame, by a lightweight technique of map-matching. Additional filtering is performed to improve the robustness of the estimation of localization.

Despite the low cost hardware, the 177 km of experimental tests demonstrated that our approach is capable of reaching high accuracy, comparable to the state-of-the-art related works (see Table I). The high accuracy was confirmed in practice through the realization of several successful autonomous trips, in conditions much more difficult than a highway. Autonomous driving still is considered a great challenge for localization systems. Only a small part of the state-of-the-art reaches this level of accuracy and, assumes the complexity and risks of such practical tests. The challenge becomes even greater if you take into account the cost.

Furthermore, the proposed approach can handle situations where the lane markings are not present or can not be detected by a short distance. That is, it does not depend directly on the existence of the lane markings in all parts of the way and no manual work is required to complete the tracks after the map is built. Nevertheless we recognize that the BLMR method needs improvements to be applicable in a more general road geometry. This is one of the goals set as future work.

Considering our future work, our main issues can be described as three topics: (i) study of alternative solutions to overcome the limitation of long straight sections; (ii) improvement of the filtering strategy; (iii) dynamic correction of the gyroscope bias; (iv) study of practical and efficient manners to create maps for a wide area.

In the case of highways, our method is not perfectly adequate, because of the long straight segments, which are very common in highways and will make the longitudinal localization error to increase, leading our algorithm to fail. One possible solution is combining the BLMR algorithm with existing lane followers. In this case, the lane follower could be activated when the longitudinal localization error is higher than a threshold value. Another possible solution is the use of more types of landmarks commonly present in standard roads. A vision algorithm capable of detecting road artifacts, like stop markings or zebra crossings, could be used to contribute to the solution of the problem of long straight sections, where the BLMR cannot perform the longitudinal localization.

We believe that the use of a more sophisticate scheme of filtering, like Bayesian filter, could lead to a more precise and robust estimation of localization. As pose measurement by BLMR (PM-BLMR) is a temporal accumulation of road surface marking detection, with its own error characteristics for each component (lateral, longitudinal and heading), an in-depth theoretical study must be performed for a proper and efficient integration with the new scheme of filtering.

Another useful issue to be treated in future are strategies to update the gyroscope bias while the vehicle is in operation. A possible solution is to use the moments when the vehicle stops, for example in a crossing with red traffic light, to make measurements of the bias. Another possible solution, is to use information from the GNSS to correct the bias while the car is moving.

In our approach, to map a wide road area, the mapping vehicle must be driven on each lane at a time, what can be a tedious and costly operation. Unfortunately, global maps vendors cannot be used because they don't have precise description of lane markings. Creation of maps from high resolution satellite images is not practical, because they don't have pixel resolution sufficient for lane marking detection. The use of aerial images from aircraft or drones can be a solution, but they are expensive and still suffer problems of occlusion in the case of tunnels, under viaducts. On the other hand, Google street view provide high resolution images, from street level, where the lane markings can be detected. We also include this as future work.

REFERENCES

[1] S. Macheng, D. Zhao, J. Sun, and H. Peng, "Improving localization accuracy in connected vehicle networks using Rao–Blackwellized particle filters: Theory, simulations, and experiments," *CoRR*, vol. abs/1702.05792, 2017. [Online]. Available: http://arxiv.org/abs/1702.05792

[2] P. D. V. Rafael, N. M. Felipe, and F. V. Raquel, "Direção autônoma baseada em visão computacional," in *XIX Congresso Brasileiro de Automática*. Campinas-SP, Brazil: Sociedade Brasileira de Automática, 2012, pp. 1430–1435.

[3] P. D. Rafael Vivacqua, N. Felipe Martins, and F. Raquel Vassallo, "Visual lane tracking and prediction for autonomous vehicles," in *Proc. Simp. Brasileiro Autom. Intel. (SBAI)*, 2013, pp. 1–7.

[4] M. Paton, F. Pomerleau, K. MacTavish, C. J. Ostafew, and T. D. Barfoot, "Expanding the limits of vision-based localization for long-term route-following autonomy," *J. Field Robot.*, vol. 34, no. 1, pp. 98–122, 2017.

[5] H. Kim, B. Liu, C. Y. Goh, S. Lee, and H. Myung, "Robust vehicle localization using entropy-weighted particle filter-based data fusion of vertical and road intensity information for a large scale urban area," *IEEE Robot. Autom. Lett.*, vol. 2, no. 3, pp. 1518–1524, Jul. 2017.

[6] J. Ziegler *et al.*, "Video based localization for bertha," in *Proc. IEEE Intell. Vehicles Symp.*, Jun. 2014, pp. 1231–1238.

[7] J. Levinson, M. Montemerlo, and S. Thrun, "Map-based precision vehicle localization in urban environments," in *Proc. Robot., Sci. Syst.*, Atlanta, GA, USA, Jun. 2007, doi: 10.15607/RSS.2007.III.016.

[8] J. Levinson and S. Thrun, "Robust vehicle localization in urban environments using probabilistic maps," in *Proc. IEEE Int. Conf. Robot. Autom. (ICRA)*, May 2010, pp. 4372–4378.

[9] M. Bertozzi, A. Broggi, E. Cardarelli, R. I. Fedriga, L. Mazzei, and P. P. Porta, "VIAC expedition toward autonomous mobility," *Robot. Autom. Mag.*, vol. 18, no. 3, pp. 120–124, Sep. 2011.

[10] J.-R. Xue, D. Wang, S.-Y. Du, D.-X. Cui, Y. Huang, and N.-N. Zheng, "A vision-centered multi-sensor fusing approach to self-localization and obstacle perception for robotic cars," *Frontiers Inf. Technol. Electron. Eng.*, vol. 18, no. 1, pp. 122–138, 2017.

[11] K. Dietmayer, N. Kämpchen, K. Fuerstenberg, J. Kibbel, W. Justus, and R. Schulz, "Roadway detection and lane detection using multilayer laserscanner," in *Advanced Microsystems for Automotive Applications*. Berlin, Germany: Springer, 2005, pp. 197–213.

[12] A. Hata and D. Wolf, "Road marking detection using LIDAR reflective intensity data and its application to vehicle localization," in *Proc. IEEE 17th Int. Conf. Intell. Transp. Syst. (ITSC)*,, 2014, pp. 584–589.

[13] S. Yang, R. Jiang, H. Wang, and S. S. Ge, "Road constrained monocular visual localization using Gaussian–Gaussian cloud model," *IEEE Trans. Intell. Transp. Syst.*, to be published. [Online]. Available: http://ieeexplore.ieee.org/document/7898840/

[14] M. Bertozzi, A. Broggi, and A. Fascioli, "VisLab and the evolution of vision-based UGVs," *IEEE Comput.*, vol. 39, no. 12, pp. 31–38, Dec. 2006.

[15] R. Gopalan, T. Hong, M. Shneier, and R. Chellappa, "A learning approach towards detection and tracking of lane markings," *IEEE Trans. Intell. Transp. Syst.*, vol. 13, no. 3, pp. 1088–1098, Sep. 2012.

[16] A. Borkar, M. Hayes, and M. T. Smith, "A novel lane detection system with efficient ground truth generation," *IEEE Trans. Intell. Transp. Syst.*, vol. 13, no. 1, pp. 365–374, Mar. 2012.

[17] G. Cui, J. Wang, and J. Li, "Robust multilane detection and tracking in urban scenarios based on LIDAR and mono-vision," *IET Image Process.*, vol. 8, no. 5, pp. 269–279, May 2014.

[18] A. Broggi, E. Cardarelli, S. Cattani, and M. Sabbatelli, "Terrain mapping for off-road autonomous ground vehicles using rational B-spline surfaces and stereo vision," in *Proc. IEEE Intell. Vehicles Symp.*, Gold Coast, QLD, Australia, Jun. 2013, pp. 648–653.
[19] F. Oniga and S. Nedevschi, "Processing dense stereo data using elevation maps: Road surface, traffic isle, and obstacle detection," *IEEE Trans. Veh. Technol.*, vol. 59, no. 3, pp. 1172–1182, Mar. 2010.
[20] H. Bay, A. Ess, T. Tuytelaars, and L. Van Gool, "Speeded-up robust features (SURF)," *Comput. Vis. Image Understand.*, vol. 110, no. 3, pp. 346–359, 2008.
[21] J. McCall and M. M. Trivedi, "Video-based lane estimation and tracking for driver assistance: Survey, system, and evaluation," *IEEE Trans. Intell. Transp. Syst.*, vol. 7, no. 1, pp. 20–37, Mar. 2006.
[22] A. B. Hillel, R. Lerner, D. Levi, and G. Raz, "Recent progress in road and lane detection: A survey," *Mach. Vis. Appl.*, vol. 25, no. 3, pp. 727–745, 2014.
[23] S. Yenikaya, G. Yenikaya, and E. Düven, "Keeping the vehicle on the road: A survey on on-road lane detection systems," *ACM Comput. Surv.*, vol. 46, no. 1, 2013, Art. no. 2.
[24] G. Kaur and D. Kumar, "Lane detection techniques: A review," *Int. J. Comput. Appl.*, vol. 112, no. 10, pp. 4–8, 2015.
[25] A. Broggi, M. Bertozzi, and A. Fascioli, "ARGO and the MilleMiglia in automatico tour," *IEEE Intell. Syst. Appl.*, vol. 14, no. 1, pp. 55–64, Jan. 1999.
[26] S.-S. Huang and L.-C. Fu, "Driver assistance system for lane detection and vehicle recognition with night vision," in *Proc. IEEE/RSJ Int. Conf. Intell. Robots Syst. (IROS)*, Aug. 2005, pp. 3530–3535.
[27] X. Miao, S. Li, and H. Shen, "On-board lane detection system for intelligent vehicle based on monocular vision," *Int. J. Smart Sens. Intell. Syst.*, vol. 5, no. 4, pp. 957–972, 2012.
[28] Y.-W. Seo and M. Hwangbo, "A computer vision system for lateral localization," *J. Field Robot.*, vol. 32, no. 7, pp. 1004–1014, 2015.
[29] G. Lu, "A lane detection, tracking and recognition system for smart vehicles," Ph.D. dissertation, School Elect. Eng. Comput. Sci., Faculty Eng., Univ. Ottawa, Ottawa, ON, Canada, 2015.
[30] O. Pink, "Visual map matching and localization using a global feature map," in *Proc. IEEE Comput. Soc. Conf. Comput. Vis. Pattern Recognit. Workshops (CVPRW)*, Jun. 2008, pp. 1–7.
[31] S. D. Pendleton *et al.*, "Perception, planning, control, and coordination for autonomous vehicles," *Machines*, vol. 5, no. 1, p. 6, 2017.
[32] H. Badino, D. Huber, and T. Kanade, "Visual topometric localization," in *Proc. IEEE Intell. Vehicles Symp. (IV)*, Jun. 2011, pp. 794–799.
[33] H. Lategahn and C. Stiller, "City GPS using stereo vision," in *Proc. IEEE Int. Conf. Veh. Electron. Safety (ICVES)*, Jul. 2012, pp. 1–6.
[34] N. Mattern, R. Schubert, and G. Wanielik, "High-accurate vehicle localization using digital maps and coherency images," in *Proc. IEEE Intell. Vehicles Symp. (IV)*, Jun. 2010, pp. 462–469.
[35] L. J. Lyrio, T. Oliveira-Santos, C. Badue, and A. F. De Souza, "Image-based mapping, global localization and position tracking using VG-RAM weightless neural networks," in *Proc. IEEE Int. Conf. Robot. Autom. (ICRA)*, May 2015, pp. 3603–3610.
[36] G. N. Desouza and A. C. Kak, "Vision for mobile robot navigation: A survey," *IEEE Trans. Pattern Anal. Mach. Intell.*, vol. 24, no. 2, pp. 237–267, Feb. 2002.
[37] H. Lategahn, M. Schreiber, J. Ziegler, and C. Stiller, "Urban localization with camera and inertial measurement unit," in *Proc. IEEE Intell. Vehicles Symp. (IV)*, Jun. 2013, pp. 719–724.
[38] D. Cui, J. Xue, and N. Zheng, "Real-time global localization of robotic cars in lane level via lane marking detection and shape registration," *IEEE Trans. Intell. Transp. Syst.*, vol. 17, no. 4, pp. 1039–1050, Apr. 2016.
[39] P. J. Besl and D. N. McKay, "A method for registration of 3-D shapes," *IEEE Trans. Pattern Anal. Mach. Intell.*, vol. 14, no. 2, pp. 239–256, Feb. 1992.
[40] B. K. P. Horn, "Closed-form solution of absolute orientation using unit quaternions," *J. Opt. Soc. Amer. A, Opt. Image Sci.*, vol. 4, no. 4, pp. 629–642, 1987.

Rafael Peixoto Derenzi Vivacqua received the B.Sc. degree in electrical engineering from the Federal University of Esprito Santo in 2001 and the M.Sc. degree in electrical engineering from the State University of Campinas 2003. He is currently pursuing the Ph.D. degree with the Electrical Engineering Faculty, Federal University of Espirito Santo, with a focus on the development of an autonomous vehicle using machine vision focusing on techniques of mapping and location. He is also a Professor with the Federal Institute of Espirito Santo, teaching analog electronics disciplines, digital electronics, microprocessors.

Massimo Bertozzi received the Ph.D. degree in information technologies from the University of Parma. He is currently an Associate Professor in computer engineering with the Dipartimento di Ingegneria dell'Informazione, University of Parma, Italy. He has been involved in different research projects to test intelligent vehicles, such as Millemiglia in Automatico in 1998, Grand Challenges in 2004 and 2005, Urban Challenge in 2007, and the VisLab Intercontinental Autonomous Challenge in 2010. His research interests are mainly focused on the application of image processing to vehicle guidance and the optimization of machine code.

Pietro Cerri received the Dr. Eng. degree in computer engineering from the Università di Pavia, Pavia, Italy, in 2003, and the Ph.D. degree in information technologies from the Università di Parma, Parma, Italy, in 2007. He is currently an Assistant Professor with the Artificial Vision and Intelligent System Laboratory, Dipartimento di Ingegneria dell'Informazione, Università di Parma. His research is mainly focused on computer vision and sensors fusion approaches for the development of advanced driver assistance systems.

Felipe Nascimento Martins received the B.Sc. M.Sc., and Ph.D. degrees in electrical engineering from the Federal University of Espirito Santo, Brazil, in 1999, 2003, and 2009, respectively. He is currently with the Institute of Engineering, Hanze University of Applied Sciences, The Netherlands, where he acts as both a Researcher and a Lecturer of electronics and robotics courses. He was involved in the organization of several robotics competitions, such as RoboCup Junior. He is involved in educational robotics. His research interests are the control of mobile robots and computer vision applied to robotics.

Raquel Frizera Vassallo received the M.Sc. degree in automation and the Ph.D. degree in electrical engineering from the Federal University of Espirito Santo (UFES), Brazil, in 1998 and 2004, respectively. Her Ph.D. dissertation was on computer vision applied to mobile robotics in cooperation with the Instituto Superior Técnico, Lisbon, Portugal. She is currently an Associate Professor with the Electrical Engineering Department, UFES. Her research is mainly focused on computer vision for mapping, robot navigation, intelligent spaces, and mobile robotics.